This is the peer-reviewed, final accepted version for American Mineralogist, published by the Mineralogical Society of America.
The published version is subject to change. Cite as Authors (Year) Title. American Mineralogist, in press.
DOI: https://doi.org/10.2138/am-2020-7606. http://www.minsocam.org/

Revision 1

Gamma-enhancement of reflected light images: a rapid, effective tool for assessment of compositional heterogeneity in pyrite

QIAOQIAO ZHU [1,2], NIGEL J. COOK [2], GUIQING XIE [3,*], CRISTIANA L. CIOBANU [4], WEI JIAN [1], BENJAMIN P. WADE[5], AND JING XU [4,6]

[1] *MNR Key Laboratory of Metallogeny and Mineral Assessment, Institute of Mineral Resources, CAGS, Beijing, 100037, China*

[2] *School of Civil, Environmental and Mining Engineering, The University of Adelaide, Adelaide, SA 5005, Australia*

[3] *Institute of Earth Science, China University of Geosciences, Beijing, 100083, China*

[4] *School of Chemical Engineering and Advanced Materials, The University of Adelaide, Adelaide, SA 5005, Australia*

[5] *Adelaide Microscopy, The University of Adelaide, Adelaide, SA 5005, Australia*

[6] *Institute of Geology and Geophysics, Chinese Academy of Sciences, Beijing, 100029, China*

ABSTRACT

Trace/minor element variation in pyrite is a feature that has proved invaluable for reconstructing a wide range of geological processes. Routine reflectance observations commonly fail to constrain this variation due to the typically subtle and barely perceptible change in reflectance brought about by deviation from ideal stoichiometry. Such differences may be difficult or impossible to observe in

[*] Corresponding author. E-mail address: xieguiqing@cags.ac.cn

Always consult and cite the final, published document. See http:/www.minsocam.org or GeoscienceWorld

This is the peer-reviewed, final accepted version for American Mineralogist, published by the Mineralogical Society of America.
The published version is subject to change. Cite as Authors (Year) Title. American Mineralogist, in press.
DOI: https://doi.org/10.2138/am-2020-7606. http://www.minsocam.org/

conventional polished sections using standard optical microscopes, at least without oil immersion. Chemical etching and staining, although widely used, are destructive and/or dangerous and the etching process is not completely reproducible. Here we use the gamma correction method to enhance optical digital signal differences obtained in reflected light in order to constrain compositional heterogeneity in pyrite from a representative hydrothermal ore deposit in eastern China. The gamma-enhanced images show significant reflectance variation caused by compositional heterogeneity, confirmed by quantitative electron microprobe analysis and qualitative imaging. Higher reflectance domains in gamma-enhanced images correspond to increases in the effective number of free electrons whereas darker domains are attributed to the decrease of these free electrons by trace/minor element substitution in pyrite (e.g., As). Gamma correction provides a rapid, effective, non-destructive method to constrain compositional heterogeneity of pyrite through enhancement of reflectance variation. Used alone, this method is unable to determine the chemical composition due to simultaneous substitutions, causing disparate increase or decrease of reflectance, in most ore minerals. Nevertheless, gamma correction may be sufficient to predict the substitution of trace/minor elements under the optical microscope prior to scanning electron microscope imaging and quantitative investigation of mineral composition and may help constrain links between textures and compositions of pyrite in evolving ore systems, which could also be applied to other ore minerals with negligible bireflectance.

Keywords: Compositional homogeneity; reflectance; pyrite; non-destructive analysis; gamma correction.

Always consult and cite the final, published document. See http:/www.minsocam.org or GeoscienceWorld

This is the peer-reviewed, final accepted version for American Mineralogist, published by the Mineralogical Society of America.
The published version is subject to change. Cite as Authors (Year) Title. American Mineralogist, in press.
DOI: https://doi.org/10.2138/am-2020-7606. http://www.minsocam.org/

INTRODUCTION

Pyrite (FeS_2) is the most common sulfide mineral in the Earth's crust and occurs in various environments ranging from low-temperature sedimentary rocks to high-temperature igneous rocks and high-grade metamorphic terrains (Craig et al. 1998). It commonly incorporates impurities (such as As, Co, Ni, Cu, and Tl) at concentrations ranging from trace levels to a few wt%. Pyrite has a refractory character and can readily retains inherited textural and compositional features during subsequent growth, making it a useful tool for ore petrologists. Applications include tracing changes of pore fluids during progressive diagenesis, tracking physicochemical conditions and enrichment mechanism of hydrothermal mineral systems, assessing trace element abundance in the oceans and atmospheric O_2 levels through geological time, as well as providing insights into the geochemical cycle of environmentally hazardous metals (such as As, Cd, Hg, and Tl) during metamorphism and weathering (Fleet et al. 1993; Craig et al. 1998; Chouinard et al. 2005; Deditius et al. 2008, 2016; Cook et al. 2013; Large et al. 2014; Gregory et al. 2015, 2019; George et al. 2018, 2019). Access to a rapid, effective way of estimating trace/minor element variation in pyrite is thus of fundamental importance for subsequent research in the field.

Prior to the ready availability of scanning electron microscope or microprobe analysis, methods widely used to constrain trace/minor element variation in pyrite include measurement of reflectance, chemical etching and staining. Reflectance is one of the major diagnostic features of ore minerals in reflected light (Ramdohr 1969; Picot et al. 1982; Criddle and Stanley 1993; Craig and Vaughan 1994). Research has established that reflectance values and reflected color of pyrite may be highly sensitive to variations in its composition even though the relationships between reflectance and impurities remain

Always consult and cite the final, published document. See http:/www.minsocam.org or GeoscienceWorld

unclear or inadequately constrained (Saager and Mihalik 1967; Vaughan 1969; Craig and Vaughan 1994). For example, the reflectance of pyrite was observed to decrease systematically with increasing of Ni and/or Co concentrations (Vaughan 1969). The variation of reflectance under reflected light is therefore expected to give clues to the substitution of trace/minor elements into pyrite, especially when pyrite concerned display compositional or growth zoning at the grain-scale. However, reflectance variation caused by compositional heterogeneity within pyrite is commonly subtle, and often invisible in conventional polished sections viewed in reflected light, at least without oil immersion (Craig 2001).

The application of chemical etching in ore mineralogy can be traced back to ~1885 and is still widely used for the textural characterization of minerals (Ramdohr 1969; Craig and Vaughan 1994; Craig 2001; Criddle 1998; Gregory et al. 2015, 2019). Some internal properties of mineral grains become visible under the optical microscope only through etching (Ramdohr 1969; Craig and Vaughan 1994). The different reaction rates between acid chemical etchants (e.g. HNO_3, HCl) and minerals result in selectively removing some domains/phases to accentuate differences between domains/phases that are otherwise near identical in optical properties (Craig and Vaughan 1994). In contrast, chemical staining, refers to the coloration attributed to optical interference by a thin surface layer of elemental sulfur generated during oxidation reactions between chemical etchants (such as H_2SO_4+KMO_4 and NaOCl) and sulfide minerals (Fleet et al. 1993). Although both methods have proven useful to expose compositional zoning, sub-grain boundaries and mineral inclusions in pyrite under reflected light (Saager and Mihalik 1967; Ramdohr 1969; Fleet et al. 1993; Craig 2001; Gregory et al. 2019; Sykora et al. 2019), they are destructive and/or dangerous and the etching process may not be completely reproducible (Craig and Vaughan 1994; Tanner et al. 2016). Furthermore, some experimentations may

Always consult and cite the final, published document. See http:/www.minsocam.org or GeoscienceWorld

be required to find the optimum conditions for acid etching and staining since the reaction rate for a certain chemical etchant may differ from mineral to mineral, or between domains within an individual mineral (Ramdohr 1969; Fleet et al. 1993).

Digital image processing technology, based on optical or scanning electron microscope (SEM) images, represents an important advance over traditional techniques in the characterization of ore minerals and underpins the technology used to carry out automatic quantitative mineral analysis and textural discrimination (Castroviejo et al. 2002; Berrezueta et al. 2016; Bachmann et al. 2017). These techniques, commonly applied to analysis of mineral processing materials, are powerful to analyze large numbers of particles and generate a great variety of information on minerals (species, size, shape, association, etc.), which would be impossible to measure accurately by manual methods (Pérez-Barnuevo et al. 2012; Berrezueta et al. 2016). Digital image processing also aims to make images easier to interpret and to increase the signal-to-noise ratio for the visualization of specific features with our unaided eyes (Heilbronner and Barrett 2014; Trauth 2015). Despite this, direct applications of digital image processing technology to constrain the compositional heterogeneity of ore minerals remain scarce. Several authors have attempted to estimate ore grade (Au, In) based on image processing and found that compositional heterogeneity might be a critical reason that led to large discrepancies between estimate data and measured bulk content (Castroviejo et al. 2002; Bachmann et al. 2017). This suggests the compositional heterogeneity induced reflectance variation could provide a major challenge for accurate mineral characterization in digital image processing (López-Benito et al. 2017).

Here we use data for pyrite from the Shizilishan Sr-(Pb-Zn) deposit, eastern China, to propose an

Always consult and cite the final, published document. See http:/www.minsocam.org or GeoscienceWorld

effective, non-destructive enhancement method to observe the compositional heterogeneity of the pyrite. The methodology is based on gamma correction of the real-time optical digital signal obtained on a petrographic microscope for mineral grains with compositional heterogeneity which can be confirmed by electron probe microanalysis (EPMA). Using the proposed technique, the observer can readily discriminate reflectance variations caused by the presence of trace/minor elements between different domains and obtain high-magnification images highlighting textures comparable with, or better than those obtained using scanning electron microscope (SEM) techniques. Indirectly, application of this new method can also provide indications of future quantitative research avenues on pyrite composition, as well as insights into ore-forming processes interpretable from ore mineral textures, when complemented by additional microbeam techniques.

BACKGROUND ON GAMMA CORRECTION

Gamma correction, also called power-law transformation, is a widely used image enhancement method which improves the interpretability or perception of information in images for human viewers (e.g., Gonzalez and Woods 2008; Maini and Aggarwal 2010; Heilbronner and Barrett 2014). The general form of the gamma correction is usually defined as:

$$s = C \cdot r^{\gamma},$$

where s and r are the gray values of output and input, respectively; C is a positive weighting constant and used to limit the gray values of s between 0 and 255, and γ is the exponent defining the gamma correction (Heilbronner and Barrett 2014). Both C and γ are built-in parameters of display equipment or software with certain ranges (Gonzalez and Woods 2008; Maini and Aggarwal 2010). These power-law transformation functions are shown graphically in Figure 1. It is obvious that the parameter

Always consult and cite the final, published document. See http:/www.minsocam.org or GeoscienceWorld

γ controls the contrast adjustment. The condition $0< \gamma<1$ produces overall contrast enhancement resulting in a brightened image and may be applied to dark images to produce brightened images. This condition is suitable for underexposed images. If $\gamma>1$, there will be contrast stretching in such a way that those gray values which are lower than the local mean will be stretched towards black (low gray values) while others are stretched towards white (high gray values) resulting in a balanced image for bright images (Vimal and Thiruvikraman 2012; Heilbronner and Barrett 2014). For example, if the input gray values are chosen as 220 and 240, we expect output values of ~67 and ~159, respectively, when using $\gamma = 10$ and $C = 2.51\times10^{-22}$ in Figure 1. In this case, the difference of input gray values is stretched from 8.33 % to 57.86 % when using higher values of γ, resulting in significant variation of gray values which is sufficient to distinguish distinct domains that originally had similar gray values.

METHODOLOGY

Pyrite-bearing samples used in this study were collected from the Shizilishan Sr-(Pb-Zn) deposit, Edong district, eastern China, which occurs at the contact between the ~139 Ma Shizilishan quartz diorite porphyry stock and Lower to Middle Triassic limestone and dolomite, as well as interlayered structures within the dolomite (Zhong 1992; Zhu et al. 2017). Lesser Pb-Zn mineralization is hosted by the dolomite, limestone, and Middle Triassic sandstone. Samples containing pyrite are from breccias. These breccias are composed of fragments of dolomite, celestite± sphalerite, and sandstone. The pyrite occurs within veins crosscutting the breccia, or as nodules near the breccia margin, with or without an association with calcite (Zhu et al. 2020).

Samples were prepared as 1-inch-diameter polished blocks and as polished thin sections. Optical and SEM observation was performed at Adelaide Microscopy (The University of Adelaide). Detailed

Always consult and cite the final, published document. See http:/www.minsocam.org or GeoscienceWorld

textural analysis on sulfides, sulfates and magnetite were performed under reflected light in air using a Nikon Eclipse LV100 POL Petrographic Microscope. Favorable areas were chosen to obtain optical digital images before and after gamma correction. Gamma correlations were refined using the Look-Up Tables (LUTs) function of the Nikon NIS-Elements D software linked to the microscope when minerals were observed at higher magnification (20X, 50X). Since ore minerals commonly have high reflectance values relative to gangue phases and also display colored reflectance (Craig and Vaughan 1994), the condition of $\gamma>1$ is employed to stretch these high gray values to make different domains more distinguishable in reflected light. A constant γ parameter of 10 was used in this study. The green channel was chosen as the principal color to display the gamma-enhanced images. Detailed operating procedures using Nikon NIS-Elements D and other types of software linked to commonly used optical microscopes are described individually in Supplementary [1] Appendix A. Following gamma enhancement, the samples were coated with carbon and examined using an FEI Quanta 450 SEM equipped with an energy-dispersive X-ray spectrometer to evaluate grain-scale compositional heterogeneity.

Quantitative mineral compositional data were obtained using a Cameca SX-Five electron probe microanalyzer. The spatial resolution was ~1 μm. Count-times were 40 s for unknowns and 8 s background for all elements. X-ray lines and standards for pyrite were: S Kα (pyrite), Pb Mα (galena), As Lα (gallium arsenide), Se Lα (Bi_2Se_3), Fe Kα (pyrite), Cu Kα (chalcopyrite), Zn Kα (sphalerite), Co Kα (cobalt), Ag Lα (silver telluride), Sb Lα (stibnite), Ni Kα (nickel olivine) and Au Lα (gold). Average minimum detection limits (mdl, wt%) were: S (0.02), Pb (0.08), As (0.05), Se (0.05), Fe (0.03), Cu

[1] Deposit item

Always consult and cite the final, published document. See http:/www.minsocam.org or GeoscienceWorld

(0.03), Zn (0.04), Co (0.03), Ag (0.05), Sb (0.04), Ni (0.03), Au (0.13). Qualitative data on compositional zoning in pyrite was obtained using a Cameca SX-Five electron probe microanalyzer. X-ray lines for pyrite were: As Lα, Co Kα, Ni Kα, Sb Lα, and Tl Mα. These elements were collected on separate spectrometers at 20 kV and 300 nA. The spatial resolution was ~0.5 µm.

RESULTS: PYRITE TEXTURES AND COMPOSITIONAL PATTERNS

Complex intergrown sulfide textures, typical of hydrothermal ores with multi-stage evolution are selected to illustrate how compositionally distinct types of pyrite can be distinguished using the optical microscope. Four sub-types of pyrite (Py1, Py2, Py3, and Py4), and two sub-types of marcasite (Mrc1, Mrc2), are recognized in Shizilishan ores based on characteristic habit, size and mutual relationships as revealed by optical observation when using gamma correction (Table 1). Comparison of images before and after gamma correction shows that it is far easier to constrain the textural relationships between distinct sub-types of pyrite and marcasite if differences in their reflectance are enhanced. The sub-types of interest here are the two pyrite sub-types (Py1 and Py3) that show contrasting grain-scale textures interpreted as representing different formation stages. An intermediate stage, with marcasite replacement of pyrite is also included for the purpose of comparison. Compositional data obtained from the coarser pyrite generations (Py1 and Py3; Table 2) shows that Py3 is arsenian, i.e., As content in the range 1.41–4.89 wt% (0.76–2.72 at%), whereas minor Co is measured in both Py1 and Py3. Otherwise, the two pyrite generations are relatively 'clean' (Table 2). A comparison between the two types of pyrite is shown on Fe *vs.* S and Fe *vs.* As plots (Fig. 2).

Pyrite 1 is clearly the earliest and has been replaced by fine-grained aggregates of marcasite (Mrc1; Fig. 3a). Small grains of Py2 occur throughout such aggregates and likely represent relicts of Py1 rather

Always consult and cite the final, published document. See http:/www.minsocam.org or GeoscienceWorld

than a separate new growth. Coarser aggregates of marcasite (Mrc2) form along veinlets or larger masses enclosing pre-existing Fe-sulfides. Relationships between these phases are clearly accentuated on the gamma-corrected images (Fig. 3b) and are poorly reproduced on BSE images (Fig. 3c) at comparable magnification. The compositional homogeneity of Py1 is well expressed on all type of images but the presence of relict Py1 within the coarser marcasite is best depicted on the reflected light image (Fig. 3a-c). This draws attention to the fact that presence of the two FeS_2 polymorphs, pyrite and marcasite, one is weakly bireflectant (marcasite) and could hinder identification using gamma-corrected images if the two minerals are intimately intergrown with one another.

In contrast, the relationships between pyrite displaying distinct textures represents an ideal case for understanding the effects of gamma correction on reflected light images. Subhedral grains of Py1 occur as preserved cores of larger aggregates of Py3 typified by fine oscillatory rhythms (colloform textures, Fig. 3d-f). The oscillatory rhythms are enhanced on the gamma-corrected images (Fig. 3e) despite their fine-scale, micron-to sub-micron rhythm widths, as resolved by BSE imaging (Fig. 3f). Moreover, the gamma-enhanced image also shows the fibrous, sectorial zoned, growth within the wider, marginal rhythms of the Py3 aggregate (Fig. 3e).

Development of more complex textures of Py3, such as coarser aggregates with oscillatory zoning overgrowing or alternating with colloform textures, is barely depicted on the reflected light image but are strongly enhanced on the gamma-corrected image, a feature replicated by chemical patterns on the BSE image (Fig. 4a-c). There is an inverse contrast between As-rich zones on gamma-corrected images and the compositional patterns on the BSE images. However, such contrast could be the cumulative effect of various elements present as traces, as suggested by the distributions of Sb and Tl on EMPA

Always consult and cite the final, published document. See http:/www.minsocam.org or GeoscienceWorld

element maps (Fig. 4d-f).

Sectorially zoned domains recognized within Py3 also display distinct oscillatory zoning patterns (Fig. 5). In one case, growth develops outside of a colloform core and sectorial zoning is only seen within the coarser outer zones (Fig. 5a-c). The gamma-corrected image reveals all the details in the growth textures and is mimicked by the compositional patterns seen on the corresponding BSE image (Fig. 5b, c). The second case (Fig. 5d-f) illustrates crystal growth with oscillatory and sectorial zoning and also displays a change in morphology from hexagonal to octagonal. The gamma-enhanced image in this case is even clearer than the BSE image (Fig. 5e, f). Such textures, with transition between different types of growth, are important for constraining distinct stages of mineralization against morphological and textural variation of pyrite.

DISCUSSION

Impurity-induced reflectance variation in ore minerals

Optical properties of ore minerals are determined by crystal chemistry, that is, by both the crystal structure (the arrangement of atoms making up the crystal) and by chemical bonding (Vaughan and Wright 1998). Based on molecular orbital/band theory, the energy of visible light is overlapped by that needed by electrons excited from the highest orbitals/valence band to empty orbitals/conduction band of a semiconductor or metal. The reflected light is expected to re-emit when the unstable excited electrons return to the ground state (Vaughan 1978; Craig and Vaughan 1994). Experiments and quantum calculations have suggested that the reflectance of semiconductors or metals will increase with the effective number of free electrons which can be excited (Burns and Vaughan 1970). For

Always consult and cite the final, published document. See http:/www.minsocam.org or GeoscienceWorld

example, the incorporation of minor/trace elements, such as Co, Ni, As and Cu, into pyrite has been shown to cause a significant decrease in reflectance (Saager and Mihalik 1967; Brown and Bartholomé 1972; Pačevski et al. 2008). This correlation was further constrained by research on the electronic structures of pyrite-type disulfides (FeS_2-CoS_2-NiS_2-CuS_2) and isochemical Pb-chalcogenides (PbS-PbSe-PbTe) (Burns and Vaughan 1970; Vaughan 1978). Bither et al. (1968) noted that the effective number of free electrons per molecule (n_{eff}, a number which reflects the electrons that can be excited by visible light incident on the surface of minerals) of pyrite-type bisulfides decreased systematically from FeS_2 to CuS_2. This led Burns and Vaughan (1970) to constrain a roughly linear correlation between N_{eff}, the effective number of free electrons per unit volume of pyrite-type bisulfides (100 $Å^3$), and their reflectance. The decrease of reflectance through isostructural pyrite-type compounds was attributed to the increase of electrons in their eg^* orbitals, into which the t_{2g} electrons can be excited, from 0 (FeS_2) to 3 (CuS_2), resulting in a decrease in the number of electrons that can be excited to re-emit light when visible light is incident on their surface. The incorporation of impurities into pyrite is therefore expected to change the effective number of free electrons on the mineral surface, causing variation in selective absorption of the incident light, and resulting in an increase or decrease of reflectance compared to the stoichiometric mineral (Craig and Vaughan 1994). It is also expected that reflectance variation will be observed at the grain or sub-grain scale when the impurity elements are not uniformly distributed in pyrite. This is due to a change of physical-chemical conditions at which precipitation takes place, subsequent replacement, and/or superposition of a new generation of hydrothermal mineralization (Vaughan 1969; Craig et al. 1998; Craig 2001; Putnis 2009; Cook et al. 2013, 2016; Ciobanu et al. 2019).

Always consult and cite the final, published document. See http:/www.minsocam.org or GeoscienceWorld

Compositional heterogeneity of pyrite from the Shizilishan deposit

The gray values of BSE images, reflecting the mean atomic mass in a given mineral are sensitive to compositional variation (Paterson et al. 1989; Craig et al. 1998; Craig 2001). Therefore, changes in the gray values on BSE images can be used as a reference for the relative enrichment or depletion of trace/minor elements in pyrite. For example, the incorporation of minor As into pyrite increases the mean atomic mass, resulting in increased brightness (higher gray values) for Py3 than Py1 in BSE images of ores from the Shizilishan deposit, as well as As-rich and As-poor domains in Py3 (Figs. 3f, 4c, d, and 5c, f). Raman analysis had demonstrated that As in Py1 and Py3 was structurally bound, causing the downshift of Raman band positions (Zhu et al. 2020).

According to the molecular orbital model, reflectance is expected to increase since the covalent character of As is stronger than S and the substitution of S by As in pyrite would delocalize electrons, resulting in increasing N_{eff} and reflectance. However, the gamma-enhanced images of pyrite demonstrate that the reflectance variation trend contrasts with the change to gray values on the BSE images (Figs. 3e, f, 4b, c, 5b, c, e, f), suggesting that As-rich domains show lower reflectance than As-poor domains in this study. Incorporation of Co and Ni is expected to decrease the reflectance of pyrite since the CoS_2 and NiS_2 has lower N_{eff} than FeS_2 (Burns and Vaughan 1970; Criddle and Stanley 1993). However, it may not be the main reason in our study case as the concentrations of Co (0.04–0.12 wt%) and Ni (mdl–0.05 wt%), as well as Sb and Tl are too low to cause such significant reflectance differences (Table 2; Fig. 4d-f). The decrease in reflectance is more likely attributable to the substitution of S by As that not only reduces the S content but also decreases the Fe content (from a mean 33.30 at% in Py1 to a mean 32.73 at% in Py3, Fig. 2), or As substituting for Fe as As^{3+} in Py3

Always consult and cite the final, published document. See http:/www.minsocam.org or GeoscienceWorld

(Deditius et al. 2008). Both changes may be expected to reduce the total number of electrons that could be excited to produce reflected light (Burns and Vaughan 1970; Vaughan 1978). This is consistent with previous observations that As, Ni, and Co-bearing pyrite, from the Free State Geduld Mine, South Africa, has a reflectance of 51.1 % at 590 nm in air, whereas relatively clean pyrite has higher reflectance of 53.2 % (Saager and Mihálik 1967). The gamma-enhanced image also demonstrates that some Py3 grains display a change in growth habit from concentric to sector zoning (Fig. 5b, e), suggesting crystallographic control on trace element incorporation, similar to the concentrically and/or sectorial-zoned auriferous pyrite reported from the high-sulfidation Au-Ag-Cu Pascua deposit, Chile-Argentina (Chouinard et al. 2005). Although reports have shown pyrite can exhibit weak bireflectance, differences in reflectance are <0.2% (Bowie 1962). The variation of reflectance of pyrite caused by impurities would thus dominate over any bireflectance, if present at all.

IMPLICATIONS FOR MINERAL CHARACTERIZATION

Compositional heterogeneity in the pyrite addressed above is expected to be expressed as reflectance variations although most are too weak to be observed under reflected light (Figs. 3d, 4a, 5a, d). Gamma correction of optical digital signals offers a rapid and effective method to reveal subtle compositional heterogeneity (Figs. 2-5). The higher reflectance domains in gamma-enhanced images correspond to an increase of effective number of free electrons whereas darker domains are attributed to relative decrease of these free electrons, compared to stoichiometric pyrite. However, variation in the relative reflectance will differ from one element to another and can be either systematically increased or decreased (as in the case of As, for example), with an increase in mean atomic mass due to minor element incorporation as indicated by BSE images. This method is, if used alone, unable to determine

Always consult and cite the final, published document. See http:/www.minsocam.org or GeoscienceWorld

chemical compositions of unknown samples, mainly due to simultaneous substitutions which cause divergent changes in reflectance (Criddle and Stanley 1993; López-Benito et al. 2017). However, a comparison of different reflectance domains under the optical microscope is generally sufficient to predict the compositional heterogeneity or provide indications about trace/minor element substitution that can be followed up by quantitative analysis (Charlat and Lévy 1976). Given that incorporation of trace elements in pyrite is almost certainly crystallographically controlled (Fig. 5b, c, e, f; Chouinard et al. 2005), gamma correction represents an alternative way to observe variations in crystal habit, which are, in turn, believed to reflect different or evolving conditions of formation (Murowchick and Barnes 1987; Alonso-Azcárate et al. 2001).

The gamma-enhanced images demonstrate clear textural evidence at the grain-scale. These are comparable to, or even clearer than the BSE images, indicating that they can also be used as additional evidence for the variation of texture, which commonly preserved the origin and growth history of pyrite (Craig 2001). Additionally, gamma correction is a non-destructive method, thus giving it clear advantages over chemical etching and staining, which are widely used in texture characterization but are destructive and/or dangerous, and may be difficult to reproduce (e.g., Fleet et al. 1993; Craig and Vaughan 1994; Craig 2001; Gregory et al. 2015, 2019; Sykora et al. 2019). Other ore minerals with negligible bireflectance, including magnetite, wolframite, and tetrahedrite, commonly display compositional heterogeneity at the grain-scale (Charlat and Lévy 1976; Craig and Vaughan 1994; Pačev ki et al. 2007; Ciobanu et al. 2019). Analogous gamma-enhanced imaging might be used to diagnose and interpret such features.

Always consult and cite the final, published document. See http:/www.minsocam.org or GeoscienceWorld

This is the peer-reviewed, final accepted version for American Mineralogist, published by the Mineralogical Society of America.
The published version is subject to change. Cite as Authors (Year) Title. American Mineralogist, in press.
DOI: https://doi.org/10.2138/am-2020-7606. http://www.minsocam.org/

ACKNOWLEDGEMENTS

This research was funded by the National Natural Science Foundation of China (41702093, 41925011), National Key Research and Development Plan (2016YFC0600206), Basic Scientific Research Operation Cost of State-Leveled Public Welfare Scientific Research Courtyard (KK1702), and China Scholarship Council (CSC, 201808110086). Special thanks are due to Senior Engineer Qingyue Hu, Shanggang Jin, and Ketao Wei (First Geological Team of Hubei Geological Bureau), Drs. Yingxiao Han and Xinhao Li (CUGB) for assistance with fieldwork and sample collection. We thank Drs. Qiuhong Hu, Abel Santos, Yinlan Ruan, and Hong Ji (University of Adelaide) for constructive discussion on the spectrometer implications. Lastly, we express our appreciation to Associate Editor Daniel Gregory, and reviewers Ross Large and Ricardo Castroviejo for their insightful comments that helped us improve this manuscript.

REFERENCES CITED

Alonso-Azcárate, J., Rodas, M., Fernández-Díaz, L., Bottrell, S.H., Mas, J.R., and López-Andrés, S. (2001) Causes of variation in crystal morphology in metamorphogenic pyrite deposits of the Cameros Basin (N Spain). Geological Journal, 36, 159–170.

Bachmann, K., Frenzel, M., Krause, J., and Gutzmer, J. (2017) Advanced identification and quantification of in-bearing minerals by scanning electron microscope-based image analysis. Microscopy and Microanalysis, 23, 527–537.

Berrezueta, E., Ordóñez-Casado, B., Bonilla, W., Banda, R., Castroviejo, R., Carrión, P., and Puglla, S. (2016) Ore petrography using optical image analysis: application to Zaruma-Portovelo deposit (Ecuador). Geosciences 6, 30.

Always consult and cite the final, published document. See http:/www.minsocam.org or GeoscienceWorld

This is the peer-reviewed, final accepted version for American Mineralogist, published by the Mineralogical Society of America.
The published version is subject to change. Cite as Authors (Year) Title. American Mineralogist, in press.
DOI: https://doi.org/10.2138/am-2020-7606. http://www.minsocam.org/

Bither, T.A., Bouchard, R.J., Cloud, W.H., Donohue, P.C., and Siemons, W.J. (1968) Transition metal pyrite dichalcogenides. High-pressure synthesis and correlation of properties. Inorganic Chemistry, 7, 2208–2220.

Bowie, S.H.U. (1962) Reflection characteristics of ore minerals. Economic Geology, 57, 983–985.

Brown, A.C., and Bartholomé, P. (1972) Inhomogeneities in cobaltiferous pyrite from the Chibuluma Cu-Co deposit, Zambia. Mineralium Deposita, 7, 100–105.

Burns, R.G., and Vaughan, D.J. (1970) Interpretation of the reflectivity behavior of ore minerals. American Mineralogist, 55, 1576–1586.

Castroviejo, R., Berrezueta, E., and Lastra, R. (2002) Microscopic digital image analysis of gold ores: a critical test of methodology, comparing reflected light and electron microscopy. Minerals and Metallurgical Processing, 19, 102–109.

Charlat, M., and Lévy, C. (1976) Influence des principales substitutions sur les propriétés optiques dans la série tennantite-tétraédrite. Bull. Soc. française Minéral. Cristallograph, 99, 29–37.

Chouinard, A., Paquette, J., and Williams-Jones, A.E. (2005) Crystallographic controls on trace-element incorporation in auriferous pyrite from the Pascua epithermal high-sulfidation deposit, Chile-Argentina. The Canadian Mineralogist, 43, 951–963.

Ciobanu, C.L., Verdugo-Ihl, M.R., Slattery, A., Cook, N.J., Ehrig, K., Courtney-Davies, L., and Wade, B.P. (2019) Silician magnetite: Si–Fe-Nanoprecipitates and other mineral inclusions in magnetite from the Olympic Dam deposit, South Australia. Minerals, 9, 311.

Cook, N.J., Ciobanu, C.L., Meria, D., Silcock, D., and Wade, B. (2013) Arsenopyrite-pyrite association in an orogenic gold ore: Tracing mineralization history from textures and trace elements. Economic Geology, 108, 1273–1283.

Always consult and cite the final, published document. See http:/www.minsocam.org or GeoscienceWorld

This is the peer-reviewed, final accepted version for American Mineralogist, published by the Mineralogical Society of America.
The published version is subject to change. Cite as Authors (Year) Title. American Mineralogist, in press.
DOI: https://doi.org/10.2138/am-2020-7606. http://www.minsocam.org/

Cook, N.J., Ciobanu, C.L., George, L., Zhu, Z.Y., Wade, B., and Ehrig, K. (2016) Trace element analysis of minerals in magmatic-hydrothermal ores by laser ablation inductively-coupled plasma mass spectrometry: Approaches and opportunities. Minerals, 6(4), 111.

Craig, J.R., (2001) Ore-mineral textures and the tales they tell. The Canadian Mineralogist, 39, 937–956.

Craig, J.R., and Vaughan, D.J. (1994) Ore Microscopy and Ore Petrography, 2nd ed., 434 p. John Wiley and Sons, Inc., New York.

Craig, J.R., Vokes, F.M., and Solberg, T.N. (1998) Pyrite: physical and chemical textures. Mineralium Deposita, 34, 82–101.

Criddle, A.J. (1998) Ore microscopy and photometry (1890–1998). In: L. Cabri, and D.J. Vaughan, Eds., Modern Approaches to Ore and Environmental Mineralogy, 27, 1–74.

Criddle, A.J., and Stanley, C.J. (1993) Quantitative Data File for Ore Minerals, 3rd ed., 635 p. Chapman and Hall / Natural History Museum, London.

Deditius, A.P., and Reich, M. (2016) Constraints on the solid solubility of Hg, Tl, and Cd in arsenian pyrite. American Mineralogist, 101, 1451–1459.

Deditius, A.P., Utsunomiya, S., Renock, D., Ewing, R.C., Ramana, C.V., Becker, U., and Kesler, S.E. (2008) A proposed new type of arsenian pyrite: Composition, nanostructure and geological significance. Geochimica et Cosmochimica Acta, 72, 2919–2933.

Fleet, M.E., Chryssoulis, S.L., MacLean, P.J., Davidson, R. and Weisener, C.G. (1993) Arsenian pyrite from gold deposits; Au and As distribution investigated by SIMS and EMP, and color staining and surface oxidation by XPS and LIMS. The Canadian Mineralogist, 31(1), 1–17.

George, L.L., Biagioni, C., D'Orazio, M. and Cook, N.J. (2018) Textural and trace element evolution of pyrite

Always consult and cite the final, published document. See http:/www.minsocam.org or GeoscienceWorld

This is the peer-reviewed, final accepted version for American Mineralogist, published by the Mineralogical Society of America.
The published version is subject to change. Cite as Authors (Year) Title. American Mineralogist, in press.
DOI: https://doi.org/10.2138/am-2020-7606. http://www.minsocam.org/

during greenschist facies metamorphic recrystallization in the southern Apuan Alps (Tuscany, Italy): influence on the formation of Tl-rich sulfosalt melt. Ore Geology Reviews, 102, 59–105.

George, L.L., Biagioni, C., Lepore, G.O., Lacalamita, M., Agrosì, G., Capitani, G.C., Bonaccorsi, E., and d'Acapito, F. (2019) The speciation of thallium in (Tl, Sb, As)-rich pyrite. Ore Geology Reviews, 107, 364–380.

Gonzalez, R.C., and Woods, R.E. (2008) Digital Image Processing, 3rd ed., 976 p. Prentice Hall International, New Jersey.

Gregory, D.D., Large, R.R., Bath, A.B., Steadman, J.A., Wu, S., Danyushevsky, L., Bull, S.W., Holden, P. and Ireland, T.R. (2016) Trace element content of pyrite from the kapai slate, St. Ives Gold District, Western Australia. Economic Geology, 111(6), 1297–1320.

Gregory, D.D., Mukherjee, I., Olson, S.L., Large, R.R., Danyushevsky, L.V., Stepanov, A.S., Avila, J.N., Cliff, J., Ireland, T.R., Raiswell, R. Olin, P.H. Maslennikov, V.V., and Lyons, T.W. (2019) The formation mechanisms of sedimentary pyrite nodules determined by trace element and sulfur isotope microanalysis. Geochimica et Cosmochimica Acta, 259, 53–68.

Heilbronner, R., and Barrett, S. (2014) Image analysis in earth sciences: microstructures and textures of earth materials. Springer-Verlag Berlin Heidelberg, Berlin.

Large, R.R., Halpin, J.A., Danyushevsky, L.V., Maslennikov, V.V., Bull, S.W., Long, J.A., Gregory, D.D., Lounejeva, E., Lyons, T.W., Sack, P.J. and McGoldrick, P.J. (2014) Trace element content of sedimentary pyrite as a new proxy for deep-time ocean–atmosphere evolution. Earth and Planetary Science Letters, 389, 209–220.

López-Benito, A., Gervilla, F., Catalina, J.C., and Castroviejo, R. (2017) Chromite typology and composition

Always consult and cite the final, published document. See http:/www.minsocam.org or GeoscienceWorld

This is the peer-reviewed, final accepted version for American Mineralogist, published by the Mineralogical Society of America.
The published version is subject to change. Cite as Authors (Year) Title. American Mineralogist, in press.
DOI: https://doi.org/10.2138/am-2020-7606. http://www.minsocam.org/

characterized through multispectral specular reflectance. Ore Geology Reviews, 89, 132–142.

Maini, R., and Aggarwal, H. (2010) A comprehensive review of image enhancement techniques. Journal of Computing, 2(3), 8–13.

Murowchick, J.B., and Barnes, H.L. (1987) Effects of temperature and degree of supersaturation on pyrite morphology. American Mineralogist, 72, 1241–1250.

Pačevski A., Götzinger, M., Dimitrijević, R. and Cvetković, L. (2007) Oscillatory zoning in wolframite from Osanica, near Bor, Serbia. Neues Jahrbuch für Mineralogie-Abhandlungen, Journal of Mineralogy and Geochemistry, 184(2), 151–160.

Pačevski A., Libowitzky, E., Zívk vić, P., Dimitrijević, R., and Cvetković, L. (2008) Copper-bearing pyrite from the Coka Marin polymetallic deposit, Serbia: Mineral inclusions or true solid-solution? The Canadian Mineralogist, 46, 249–261.

Paterson, B.A., Stephens, W.E., and Herd, D.A. (1989) Zoning in granitoid accessory minerals as revealed by backscattered electron imagery. Mineralogical Magazine, 53, 55–61.

Pérez-Barnuevo, L., Pirard, E., and Castroviejo, R. (2012) Textural descriptors for multiphasic ore particles. Image Analysis & Stereology, 31, 175–184.

Picot, P., Johan, Z., and Watkinson, D.H. (1982) Atlas of Ore Minerals, Elsevier.

Putnis, A. (2009) Mineral replacement reactions. Reviews in Mineralogy and Geochemistry, 70(1), 87–124.

Ramdohr, P. (1969) The Ore Minerals and Their Intergrowths,1st ed., 1174 p. Pergamon Press, London.

Saager, R., and Mihalik, P. (1967) Two varieties of pyrite from the Basal Reef of the Witwatersrand System. Economic Geology, 62, 719–731.

Sykora, S., Cooke, D.R., Meffre, S., Stephanov, A.S., Gardner, K., Scott, R., Selley, D., and Harris, A.C. (2018)

Always consult and cite the final, published document. See http:/www.minsocam.org or GeoscienceWorld

This is the peer-reviewed, final accepted version for American Mineralogist, published by the Mineralogical Society of America.
The published version is subject to change. Cite as Authors (Year) Title. American Mineralogist, in press.
DOI: https://doi.org/10.2138/am-2020-7606. http://www.minsocam.org/

Evolution of pyrite trace element compositions from porphyry-style and epithermal conditions at the Lihir gold deposit: Implications for ore genesis and mineral processing. Economic Geology, 113, 193–208.

Tanner, D., Henley, R.W., Mavrogenes, J.A. and Holden, P. (2016) Sulfur isotope and trace element systematics of zoned pyrite crystals from the El Indio Au–Cu–Ag deposit, Chile. Contributions to Mineralogy and Petrology, 171(4), 33.

Trauth, M.H. (2015) MATLAB® Recipes for Earth Sciences, 4th ed., 427 p. Springer, Berlin.

Vaughan, D.J. (1969) Zonal variation in bravoite. American Mineralogist, 54, 1075–1083.

Vaughan, D.J. (1978) The interpretation and prediction of the properties of opaque minerals from crystal chemical models. Bulletin de Minéralogie, 101, 484–497.

Vaughan, D.J., and Wright, K.V. (1998) Crystal chemistry of arsenic minerals. In: L. Cabri, and D.J. Vaughan, Eds., Modern Approaches to Ore and Environmental Mineralogy, 27, 75–109.

Vimal, S.P., and Thiruvikraman, P.K. (2012) Automated image enhancement using power law transformations. Sādhanā, 37, 739–745.

Zhong, G.H. (1992) Geological characteristics and ore genesis of the Shizilishan celestite deposit, Huangshi: Geological Science and Technology Information of Hubei, (2), 35–41(in Chinese).

Zhu, Q.Q., Xie, G.Q., and Han, Y.X. (2017) SHRIMP zircon U-Pb dating of quartz diorite porphyry from the Shizilishan Sr (Pb-Zn) deposit in Hubei Province and its geological significance. Acta Petrologica Sinica, 33, 3484–3494 (in Chinese with English abstract)

Zhu, Q.Q., Cook, N.J., Xie, G.Q., Wade, B.P., and Ciobanu, C.L. (2020) Arsenic-induced downshift of Raman band positions for pyrite. Economic Geology, in press.

Figure captions

Always consult and cite the final, published document. See http:/www.minsocam.org or GeoscienceWorld

Fig. 1. Plot of gamma correction result for various γ using different values of constant C to scale each curve to fit the range shown, where s and *r* are the gray values of output and input, respectively. Figure modified after Gonzalez and Woods (2008) and Vimal and Thiruvikraman (2012).

Fig. 2. Binary plots of (a) Fe *vs.* S, (b) Fe *vs.* As of EMPA data in Py1 and Py3, expressed in atomic percent (at%).

Fig. 3. Reflected light (a and d), gamma-enhanced (b and e) and BSE images (c and f) showing textural relationship between generations of pyrite. (a–c) Euhedral Py1 included within fine-grained, spongy aggregates of Py2+Mrc1 which are crosscut by coarser, vein-like Mrc2. In reflected light, Py1 shows a brownish color when surrounded by aggregates of Py2+Mrc1. (d–f) Py3 observed as colloform overgrowths on Py1 which is also crosscut by galena+Py3. Boundaries between sub-types of pyrite and marcasite are marked by white dashed lines in (b) and (e). Abbreviation: Mrc−marcasite; Py−pyrite; Gn−galena.

Fig. 4. Shift in the growth habit and compositional zonation of Py3. Euhedral grains of Py1 preserved as cores within Py3 featuring fine oscillatory rhythmic zoning which gradually changes to growth zoning combined with sectorial zoning. The shift is clearly demonstrated in the gamma-enhanced (b) and BSE image (c) but is only faintly seen under reflected light image (a). Zoning in Py3 is also revealed by variation in the contents of As (d), Sb (e) and Tl (f). Boundary between Py1 and Py3 marked by white dashed lines in the gamma-enhanced image (b). Abbreviation: Py−pyrite.

Fig. 5. Growth habit of Py3 changes from an oscillatory-zoned core to a sectorial-zoned rim. The sector zoning displayed in the gamma-enhanced image (b, e) may actually be clearer compared to the BSE image (c, f). a, d−Reflected light image. Abbreviation: Py–pyrite.

Always consult and cite the final, published document. See http:/www.minsocam.org or GeoscienceWorld

This is the peer-reviewed, final accepted version for American Mineralogist, published by the Mineralogical Society of America.
The published version is subject to change. Cite as Authors (Year) Title. American Mineralogist, in press.
DOI: https://doi.org/10.2138/am-2020-7606. http://www.minsocam.org/

Table 1. Summary of features of pyrite and marcasite from the Shizilishan Sr-(Pb-Zn) deposit.

Sub-types	Py1	Mrc1	Py2	Mrc2	Py3	Py4
Reflected color	yellow-white, appears brownish when surrounded by Mrc2 or Mrc1+Py2	greenish-gray to weak brown-white	yellow-white but slightly whiter than Py1	greenish and bluish grays to brown-white	yellow-white to pinkish-grey	yellow-white
Crystal size	10~50 μm	<2 μm	<2 μm	5~35 μm	20~>100 μm	2~5 μm
Growth habit	euhedral, discrete grains, some grains displays concentric, porous core and gradually changes to euhedral surface	aggregates to form spongy texture	aggregates to form spongy texture	anhedral or lath-like crystals	anhedral to euhedral morphology, changes from colloform core to growth zones in rim or from oscillatory-zoned core to sectorial-zoned rim	anhedral aggregates to form veins
Intergrowth relationships	overgrown by later pyrite and marcasite	replacing and overgrowing Py1	likely relicts of Py1 replaced by Mrc1	crosscut or overgrown on Py2+Mrc1 aggregates	overgrown on Py1, Py2+Mrc1 and Mrc2; crosscut Py1 sometimes	crosscut Py3 or cemented broken Py3 crystal

Notes: Py−pyrite; Mrc−marcasite.

Always consult and cite the final, published document. See http:/www.minsocam.org or GeoscienceWorld

This is the peer-reviewed, final accepted version for American Mineralogist, published by the Mineralogical Society of America.
The published version is subject to change. Cite as Authors (Year) Title. American Mineralogist, in press.
DOI: https://doi.org/10.2138/am-2020-7606. http://www.minsocam.org/

Table 2. Electron microprobe data for pyrite (wt%) and minimum detection limits.

Sample	Minimum detection limit	SL2-1 B2-1						SL14-1 C3-1-5									SL14-1 C3-1-7		
		1	2	12	13	14	17	1	2	3	4	5	7	8	8-1	9	6	7	8
Sub-type		Py1	Py1	Py1	Py1	Py1	Py1	Py1	Py1	Py1	Py3	Py3	Py3	Py3	Py3	Py3	Py3	Py3	Py3
S	0.02	53.28	53.04	53.01	52.11	53.03	52.83	53.60	53.30	52.46	50.81	50.25	50.48	52.04	51.68	51.13	50.00	51.81	52.09
As	0.05	<	0.07	<	<	0.06	<	0.12	0.07	0.45	3.90	4.25	4.65	1.77	1.93	3.03	4.89	1.62	1.41
Se	0.05	<	<	<	<	<	<	<	<	<	<	<	<	<	<	0.05	0.07	<	<
Fe	0.03	46.32	46.28	46.21	45.86	46.51	46.44	46.13	46.18	45.71	43.94	43.62	43.43	45.37	45.31	44.55	43.38	45.32	45.69
Cu	0.03	<	<	<	0.04	<	<	<	<	<	<	<	<	<	<	<	<	<	<
Co	0.03	0.04	0.12	0.06	0.06	0.04	0.10	0.07	0.07	0.06	0.07	0.04	0.07	0.07	0.04	0.08	0.07	0.06	0.08
Sb	0.04	<	<	<	<	<	<	<	<	<	<	<	<	<	<	<	0.04	<	<
Ni	0.03	<	<	<	0.05	<	<	<	0.04	<	<	<	<	<	<	<	<	<	<
Total		99.80	99.61	99.35	98.20	99.68	99.54	99.99	99.71	98.70	98.85	98.25	98.74	99.26	99.05	98.88	98.51	98.91	99.34
		Calculated atomic percent (at%)																	
S		66.64	66.52	66.59	66.34	66.46	66.38	66.82	66.69	66.45	65.33	65.12	65.14	65.97	65.78	65.47	64.86	65.92	65.94
As		<	0.04	<	<	0.03	<	0.07	0.04	0.25	2.14	2.35	2.57	0.96	1.05	1.66	2.72	0.88	0.76
Se		<	<	<	<	<	<	<	<	<	<	<	<	<	<	0.03	0.04	<	<
Fe		33.26	33.32	33.33	33.51	33.47	33.50	33.02	33.17	33.24	32.44	32.46	32.18	33.01	33.11	32.76	32.30	33.11	33.21
Cu		<	<	<	0.02	<	<	<	<	<	<	<	<	<	<	<	<	<	<
Co		0.03	0.08	0.04	0.04	0.03	0.07	0.05	0.05	0.04	0.05	0.03	0.05	0.05	0.03	0.05	0.05	0.04	0.06
Sb		<	<	<	<	<	<	<	<	<	<	<	<	<	<	<	0.01	<	<
Ni		<	<	<	0.03	<	<	<	0.03	<	<	<	<	<	<	<	<	<	<

Notes: Py−pyrite; <−below minimum limit of detection; All data for Pb, Zn, Ag, and Au are below minimum detection limit and are thus not show here.

Always consult and cite the final, published document. See http:/www.minsocam.org or GeoscienceWorld

This is the peer-reviewed, final accepted version for American Mineralogist, published by the Mineralogical Society of America.
The published version is subject to change. Cite as Authors (Year) Title. American Mineralogist, in press.
DOI: https://doi.org/10.2138/am-2020-7606. http://www.minsocam.org/

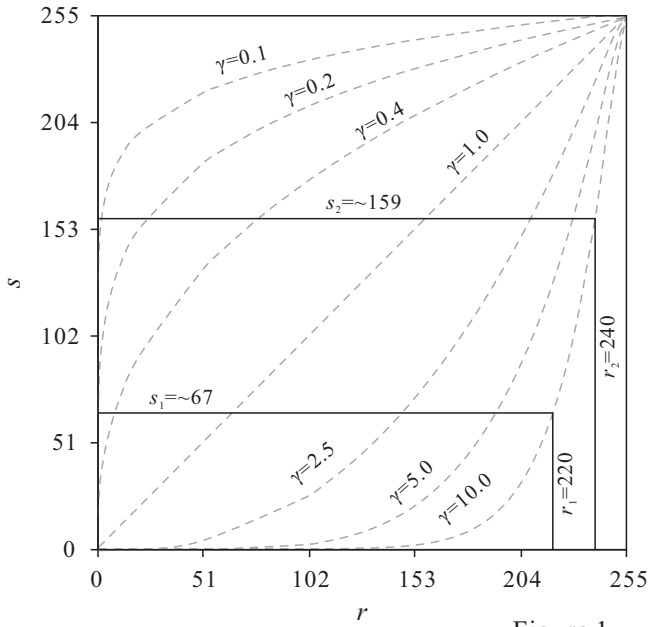

Figure 1

Always consult and cite the final, published document. See http:/www.minsocam.org or GeoscienceWorld

This is the peer-reviewed, final accepted version for American Mineralogist, published by the Mineralogical Society of America.
The published version is subject to change. Cite as Authors (Year) Title. American Mineralogist, in press.
DOI: https://doi.org/10.2138/am-2020-7606. http://www.minsocam.org/

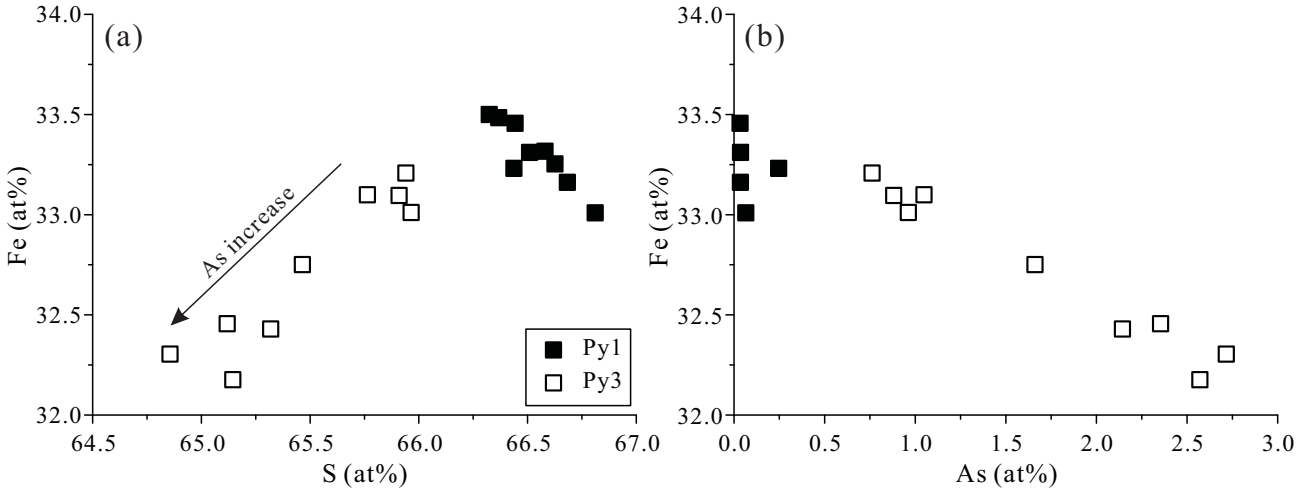

Figure 2

Always consult and cite the final, published document. See http:/www.minsocam.org or GeoscienceWorld

This is the peer-reviewed, final accepted version for American Mineralogist, published by the Mineralogical Society of America.
The published version is subject to change. Cite as Authors (Year) Title. American Mineralogist, in press.
DOI: https://doi.org/10.2138/am-2020-7606. http://www.minsocam.org/

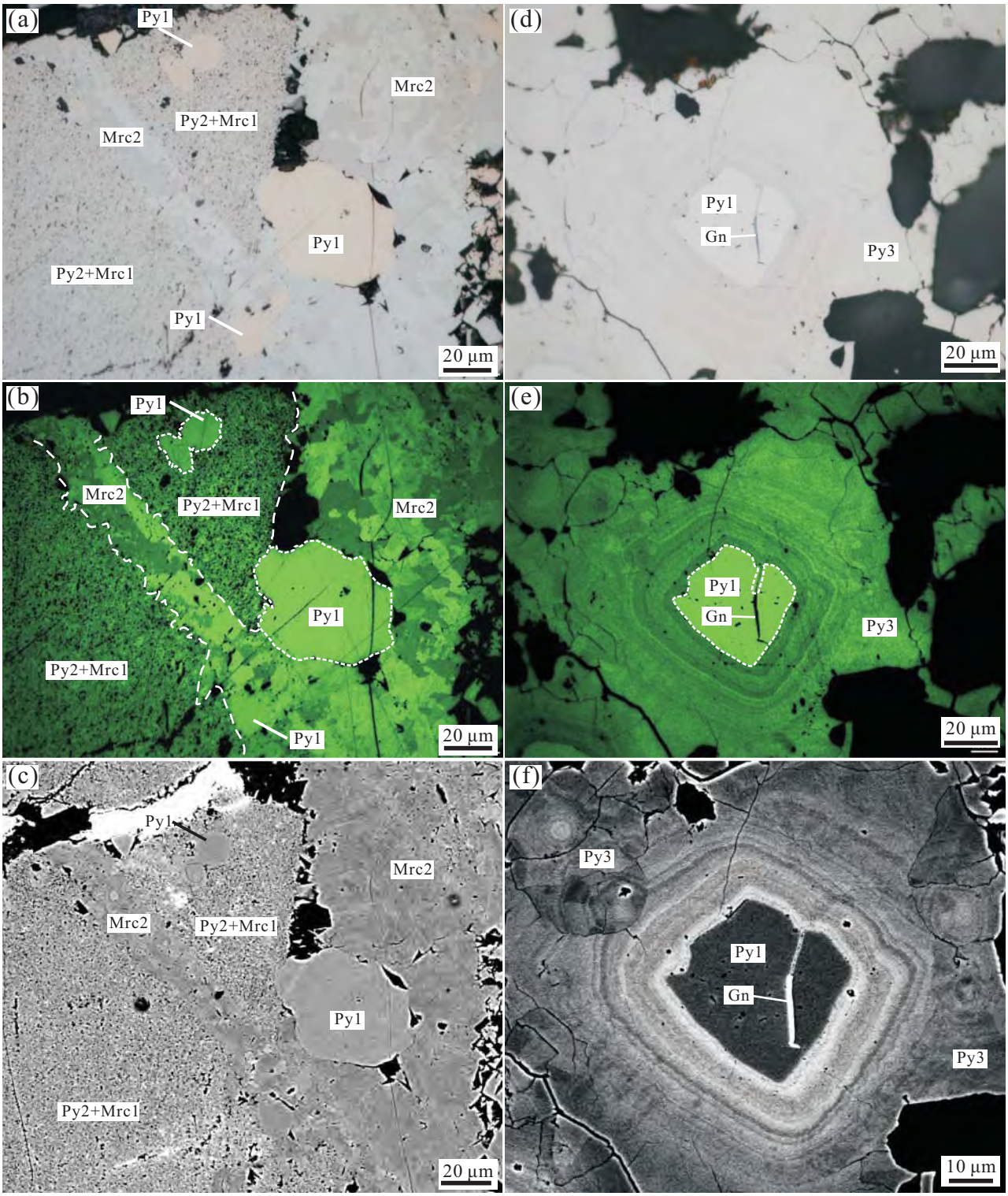

Figure 3

Always consult and cite the final, published document. See http:/www.minsocam.org or GeoscienceWorld

This is the peer-reviewed, final accepted version for American Mineralogist, published by the Mineralogical Society of America.
The published version is subject to change. Cite as Authors (Year) Title. American Mineralogist, in press.
DOI: https://doi.org/10.2138/am-2020-7606. http://www.minsocam.org/

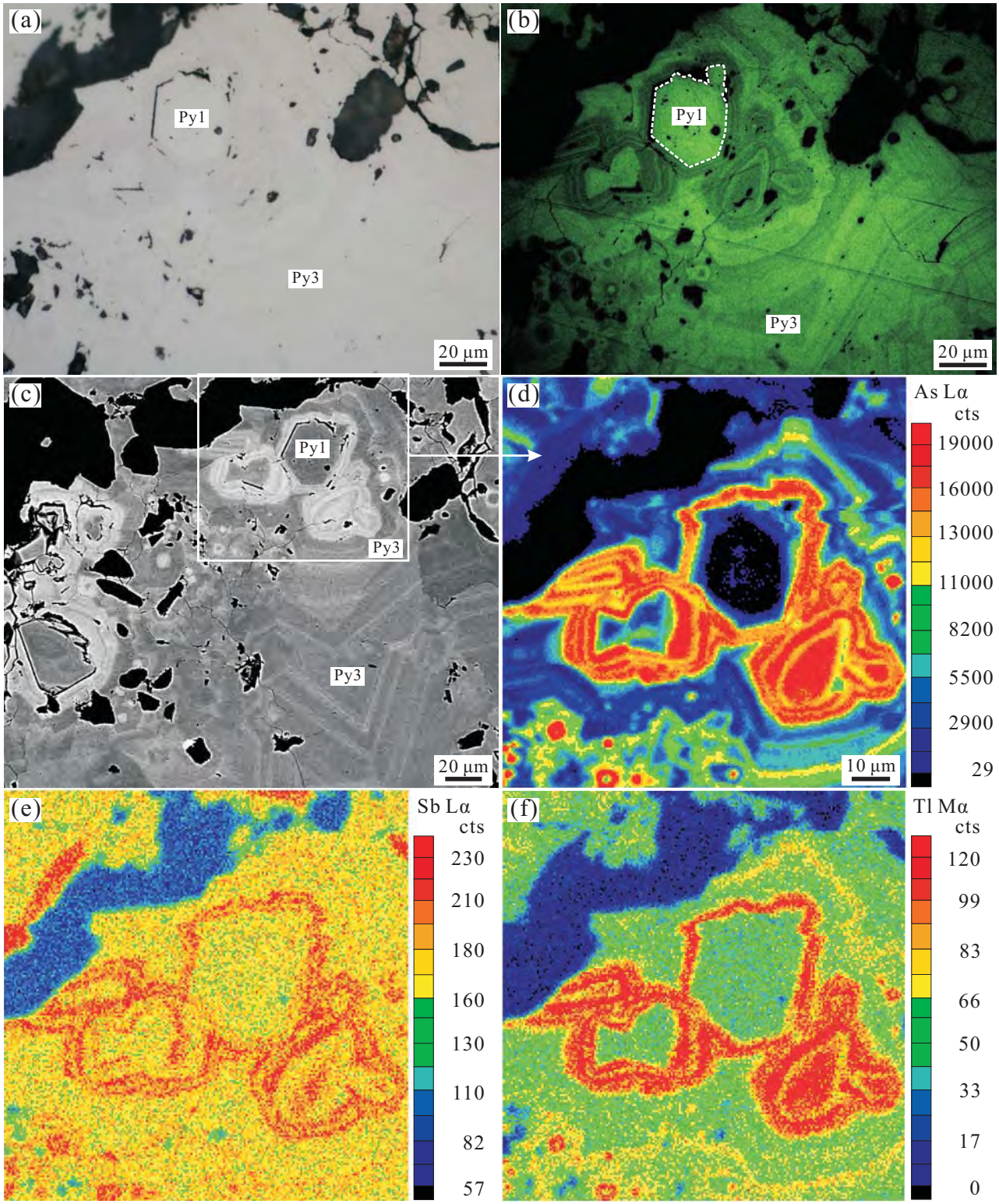

Figure 4

Always consult and cite the final, published document. See http:/www.minsocam.org or GeoscienceWorld

This is the peer-reviewed, final accepted version for American Mineralogist, published by the Mineralogical Society of America.
The published version is subject to change. Cite as Authors (Year) Title. American Mineralogist, in press.
DOI: https://doi.org/10.2138/am-2020-7606. http://www.minsocam.org/

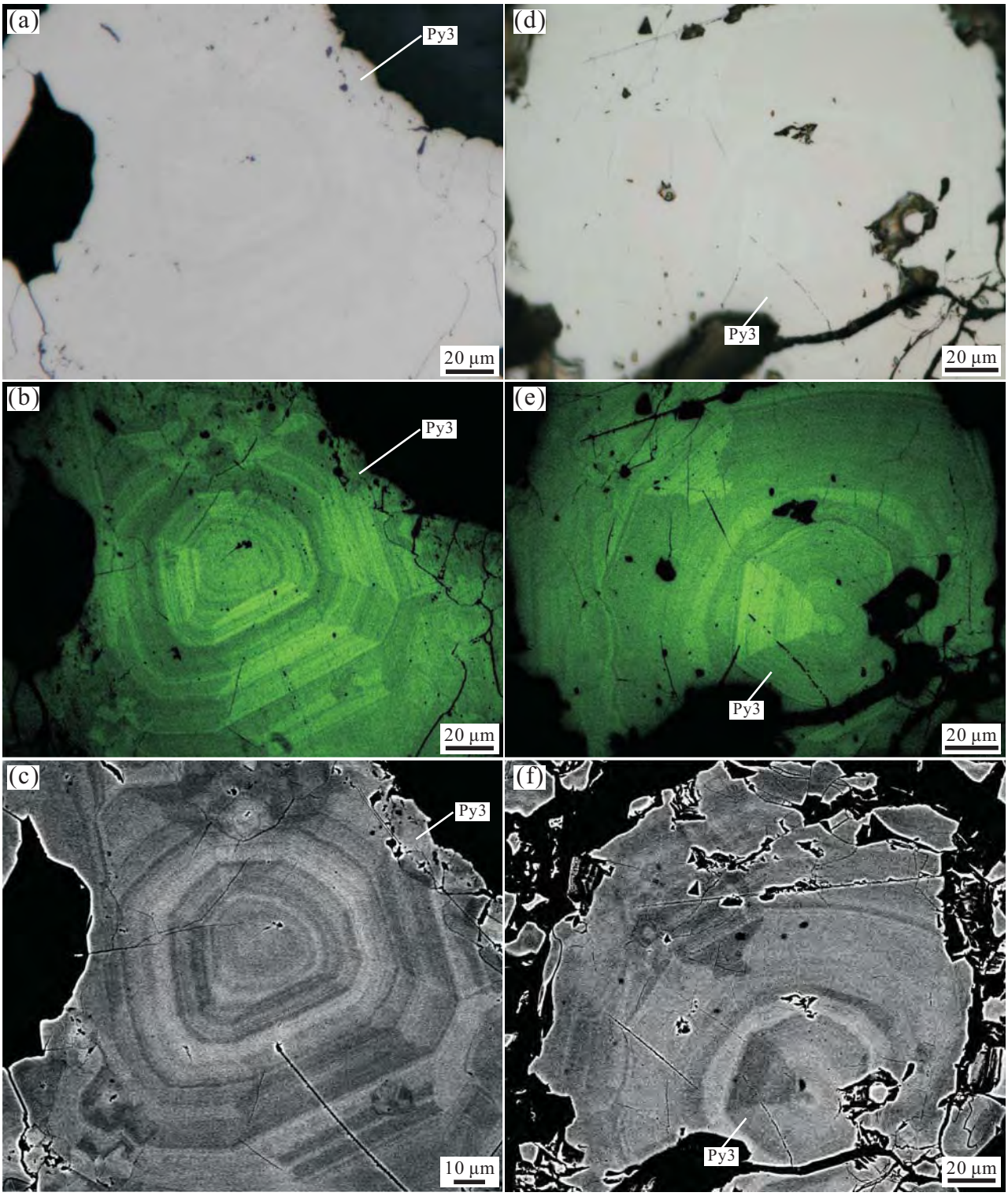

Figure 5

Always consult and cite the final, published document. See http:/www.minsocam.org or GeoscienceWorld